

Ego-Motion Estimation and Dynamic Motion Separation from 3D Point Clouds for Accumulating Data and Improving 3D Object Detection

Patrick Palmer, TU Dortmund, Institute of Control Theory and Systems Engineering, 44227 Dortmund, patrick.palmer@tu-dortmund.de

Martin Krüger, TU Dortmund, Institute of Control Theory and Systems Engineering, 44227 Dortmund, martin2.krueger@tu-dortmund.de

Dr. Richard Altendorfer, ZF Group, 56070 Koblenz, richard.altendorfer@zf.com

Univ.-Prof. Dr.-Ing. Prof. h.c. Dr. h.c. Torsten Bertram, TU Dortmund, Institute of Control Theory and Systems Engineering, 44227 Dortmund, torsten.bertram@tu-dortmund.de

Abstract

New 3+1D high-resolution radar sensors are gaining importance for 3D object detection in the automotive domain due to their relative affordability and improved detection compared to classic low-resolution radar sensors. One limitation of high-resolution radar sensors, compared to lidar sensors, is the sparsity of the generated point cloud. This sparsity could be partially overcome by accumulating radar point clouds of subsequent time steps. This contribution analyzes limitations of accumulating radar point clouds on the View-of-Delft dataset [1]. By employing different ego-motion estimation approaches, the dataset's inherent constraints, and possible solutions are analyzed. Additionally, a learning-based instance motion estimation approach is deployed to investigate the influence of dynamic motion on the accumulated point cloud for object detection. Experiments document an improved object detection performance by applying an ego-motion estimation and dynamic motion correction approach.

1 Introduction

One of the critical challenges of automating vehicles and the driving process is the perception of the environment. Precise knowledge of the traffic scene is necessary to make well-informed decisions on the automated vehicle's path planning and react adequately to sudden actions of other traffic participants. False, missing or imprecise detections entail errors in the environment model. This increases the risk of accidents and limits the time horizon for safe and comfortable vehicle path planning. Different sensor modalities are utilized in research and production vehicles for environment perception. Research vehicles mainly use high-resolution lidars due to their high information density and accuracy, whereas series production vehicles primarily use low-cost sensors like radars and cameras. An emerging sensor technology that is supposed to bridge the gap between lidar and traditional low-resolution radar sensors are 3+1D high-resolution radar sensors. Compared to traditional radars, these high-resolution radar sensors also measure the elevation angle and generate a denser point cloud while preserving the advantages of radar sensors like the direct estimation of the relative radial velocity v_{rr} , robustness against adverse weather conditions, and relatively low cost. Despite improvements in radar technology, currently available 3+1D radar sensors still suffer from noisy measurements and relatively sparse point clouds (compared to lidar). These limitations constrain the perception performance and thus affect the following modules (and their performance) in an automated driving stack. A common strategy to overcome the sparsity of low-resolution lidar and

radar point clouds is the aggregation of information over concurrent time steps by accumulation. This yields a denser point cloud that can be used for perception tasks like 3D object detection. For static objects, an accumulation can be done by transforming point positions from the previous to the current coordinate frame using the ego-motion alone. Nowadays, ego-motion is mostly estimated by combining GPS, wheel odometry, and inertial measurements (angular rates and accelerations) and is available for most public datasets. Targets from dynamic objects, such as reflections from cars, pedestrians, and cyclists, must be considered separately. A naive accumulation of these points based on the ego-motion alone results in an error, represented by trailing points behind the object. An example can be seen in Fig. 1, the bicycle on the bottom left (ID: VIII) has a tail of points outside the bounding box. Due to the radar sensor's direct measurement of radar radial velocity v_{rr} , an accurate distinction between static and dynamic points is possible [2]. The v_{rr} can additionally be used for estimating the velocity over ground of objects. Considering the motion of dynamic objects when accumulating point clouds from subsequent frames leads to improved consistency of the accumulated point cloud. Hence, the accuracy of object detection approaches applied to the point cloud increases [3].

Related Work: For lidar [4, 5] and 3+1D high-resolution radar data [6] flow-based methods, that only utilize the point coordinates, can accurately estimate the scene flow for a point cloud. The point cloud can be separated into static and dynamic areas using the scene flow. Static points can then be used to estimate the ego-motion, while the

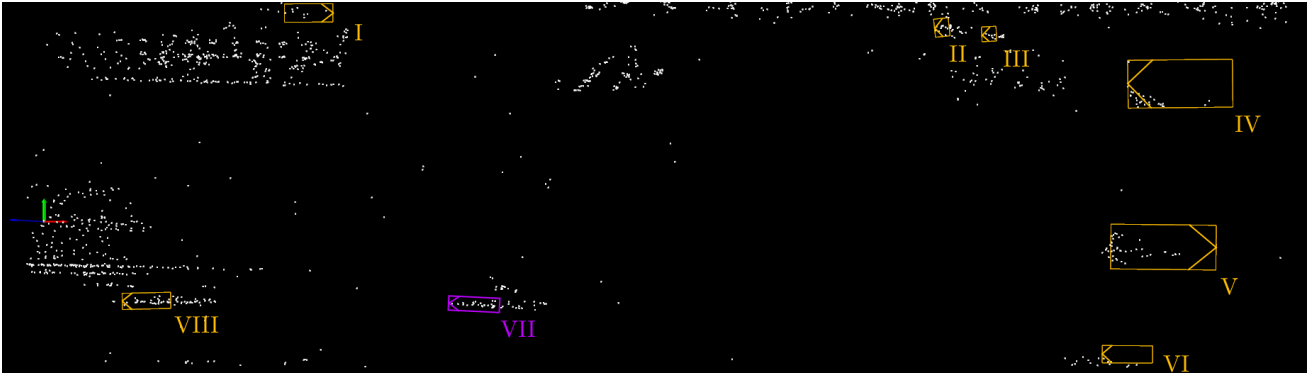


Figure 1 Bird’s eye view perspective of a traffic scene visualizing an aggregated point cloud, accumulated over five frames. The ego-vehicle is located on the left, represented by the colored coordinate system indicating the sensor mounting position (viewing towards the right). Orange boxes represent annotated ground truth bounding boxes and the purple rectangle indicates a manually added ground truth bounding box. The roman numerals mark the objects identifier (ID). The arrow represents the direction of motion.

instance’s motion can be derived from the dynamic points. By extending the considered time horizon and employing motion segmentation [7] (PCAc) has shown that accurate accumulation of point clouds is possible given only the naively accumulated point clouds.

As summarized by [8], multiple 3+1D radar datasets have been proposed, each suffering from unique limitations, making most of them unfeasible for the ultimate goal of 3D object detection. The View-of-Delft (VoD) dataset [1] meets the requirements. It provides time-continuous labeled objects, non-accumulated radar data, and additional sensor modalities like high-resolution lidar and camera sensor data. The main contributions of the work at hand are:

- Evaluating ego-motion estimation approaches to accumulate high-resolution radar point clouds on subsequent frames on the VoD dataset.
- Adaptation of PCAc [7] approach to the VoD dataset and evaluation of the transferability to radar data.
- Investigating the influence of different dynamic and static motion correction approaches on the performance of 3D object detection.

2 Limitations of the VoD dataset

The VoD dataset is one of very few datasets that include 3+1D high-resolution radar measurements. In addition to the radar sensor, mono camera and high-resolution 64-layer lidar data are provided. Due to the dataset’s focus on urban scenarios where different types of traffic participants share the same space, only a limited view range of up to 51.2m is considered, and the amount of observed pedestrians and cyclist is high compared to other datasets like the Astyx dataset [9]. One major limitation of the dataset is the accuracy of labeled objects. Multiple objects are either not labeled or mislabeled. An example is visualized in Fig. 1. In the lower part of the image are three bicycles. The foremost one (ID: VIII) is labeled correctly. The middle one (ID: VII) is not labeled at all, and the label for the sternmost one (ID: VI) is not well aligned to the cluster of close

targets. The questionable quality of such annotations negatively influences the training because misaligned or missing annotations confuse the training procedure. Due to the time and effort necessary for correcting annotations, only minor label adaptations have been applied to mitigate the problem of object reflection points that lay outside the bounding box. The box is extended by 0.2 m in each direction to capture most of the points belonging to an object, similar to [10]. The second observed limitation is the unavailability of ground truth ego-motion information. The authors provide an accumulated set of radar scans but do not provide the utilized ego-motion for generating them. This limits the ability to investigate dynamic object motion. Additionally, the reproduction of the accumulated scans is hindered by different sampling frequencies of the radar sensor and the provided single radar scans. The utilized sensor captures the scene with a frequency of 13 Hz, but the single-frame data is only provided with a frequency of 10 Hz, to synchronize the measurement of the radar to the other sensor modalities. The provided accumulated point cloud is collected from the base 13 Hz data. Certain radar scans are therefore not provided and the time interval between the provided frames varies. Different strategies of estimating ego-motion are investigated in the following chapter to mitigate the missing ego-motion information.

Ego-Motion Estimation

The ego-vehicle motion is described as a transformation matrix that consists of the translation and rotation of the ego-vehicle between two consecutive time steps. It can be derived either from an inertial measurement-based system or directly from environmental measurement sensors.

Ego-Motion-Estimation from Pose (EM-P): The VoD dataset does not directly provide information about the ego-motion. However, transformation matrices from the camera coordinate system to a *map* and a *world* coordinate system are provided. Both transformations only differ in the definition of the point of origin. Hence, the ego-motion is calculated from the transformation between consecutive frames.

Ego-Motion-Estimation from Point Cloud with GICP

(EM-G): Due to limitations observed in the ego-motion from the VoD pose estimation, a method for estimating the motion directly from the recorded point cloud is investigated. Generalized Iterative Closest Point (GICP)[11] is chosen due to its simple implementation and the assumed sufficient accuracy. It is applied to the lidar and high-resolution radar point cloud separately.

Averaging of estimated motion over multiple time steps (EM-mG): Due to the high oscillation of the EM-G output, as can be seen in Fig. 2, an averaging of the transformation matrix is employed to reduce implausible fluctuations. The average of the translation and rotation matrices are calculated separately. Due to an observed pattern that repeats every 6 time steps, the translation is averaged by calculating the moving average over the translation at 6 consecutive time steps. An averaging of the rotation matrix is not trivial. One way of averaging utilized in this work is to transform the rotation matrix into a quaternion representation. Then, the average quaternion is calculated using singular value decomposition (SVD) [12], over the same 6 consecutive time steps. Afterward, the quaternion is re-transformed into the rotation matrix.

Estimation from measured radar radial velocity (EM- v_{rr}): One unique feature of the radar point cloud that can be utilized to estimate ego-motion is the direct measurement of v_{rr} . The ego-motion can be estimated by applying a least squares-based approach to the static points in the scene, as described in [13]. The main difference to alternative approaches is, that only measurements from a single frame are needed. The differentiation of static and dynamic points is done by estimating the static points using a random sample consensus algorithm [14]. Due to the additional information about the elevation angle ε measured by the 3+1D radar sensor, the observation angle φ is utilized, instead of the azimuth angle ϑ . Calculated using the spherical Pythagorean theorem:

$$\varphi = \cos^{-1}(\cos(\vartheta)\cos(\varepsilon)) \quad (1)$$

Estimation from static objects (EM-SO): The VoD dataset includes labels and track identifiers for some static objects like *bicycle racks* and *unused bicycles*. The track identifiers enable the re-identification of objects in consecutive frames. Assuming noise-free data, the rotation R and translation t can be derived by solving:

$$RC_{k-1} + t = C_k \quad (2)$$

Where C represents the center points of all objects at time step $k - 1$ and k . Due to noise in the data, a least squares-based approach is used to derive the motion. Unfortunately, static objects do not occur in every frame. That limits the usefulness and accuracy of this method significantly and also makes it dependent on the accuracy of the annotation of static objects. Hence, this approach is only considered as a baseline for comparing the previous methods against.

3 Treatment of Dynamic Objects

Due to the motion of certain objects an accumulation of the point cloud by just considering ego-motion results in an error for moving objects. For the foremost bicycle on the

bottom left in Fig. 1, this is represented by the smearing pattern of points behind the object. This negatively influences the training as objects get represented differently depending on their motion.

Estimation from the provided labels (Dyn-GT): For a baseline approach the motion of objects can be derived from the labels by estimating the transformation between the center points of objects. This is the best-case baseline to which the other approaches will be compared.

Relative Radial Velocity (Dyn- v_{rr}): If an object only moves in a radial direction to the radar sensor, the full motion of the object can be measured accurately. Unfortunately, objects rarely just move in radial direction, which limits this approach. Nevertheless, a correction by v_{rr} will result in a good motion correction for all vehicles that move in the same or opposite direction to the ego-vehicle.

Learning-Based Estimation of Dynamic Motion (Dyn-PCAc): To directly estimate the dynamic object motion from the point cloud, PCAc [7] is adapted to the VoD dataset. PCAc [7] is a supervised end-to-end learning-based algorithm that first estimates the ego-motion (EM-PCAc) of the vehicle by separating the scene into static and dynamic areas and employing robust point matching on the static points. Afterward, motion segmentation and instance association steps are executed to derive the instance motion and correct the point's position in the accumulated point cloud. When using the estimated ego-motion and the labels of dynamic objects, a ground truth motion set can be derived. This is used during training.

4 Experimental Evaluation

For the overall goal of improving the object detection performance the evaluation of the accuracy of the ego-motion estimation as well as the instance motion assignment are analyzed by investigating their influence on the object detection performance. PointPillars [15] is used as the 3D object detection method as implemented in the OpenPCDet framework [16]. Minor adaptations to the model configuration were made, as described by [1]. PointPillars is chosen over other object detectors due to its popularity for radar-based perception methods, see e.g. [1]. In previous investigations [17] it has shown to provide at least comparable, if not better detection performance than other detectors while also being computationally efficient.

Training Details: All experiments are carried out with three different reproducible model initializations to reduce performance dependencies on the initialization. The model is trained for at most 125 epochs utilizing a one-cycle learning rate scheduler [18]. Due to observations that the bulk of training progress happens at low learning rates, the learning rate scheduler is adapted to spend more time at lower learning rates while preserving the one-cycle character. For the VoD test set no labels are provided as the authors intend to provide an evaluation server later, similar to the KITTI dataset [19]. Hence, we used the validation set for evaluation.

Evaluation Metrics: Similar to KITTI [19] and [1], we use Average Precision (AP) as the primary performance metric but require a higher minimum intersection over union

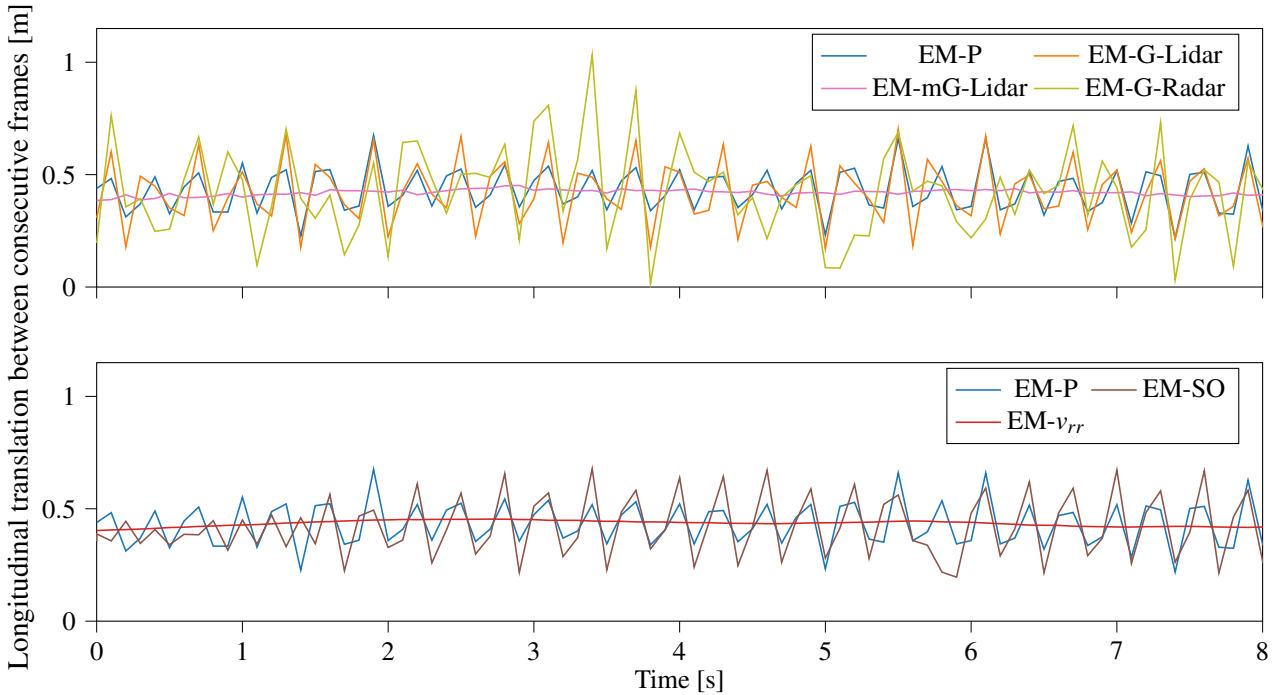


Figure 2 Translation between frames in driving direction estimated from various sensor modalities for an exemplary scene with an approximately constant velocity of 15 km h^{-1} in driving direction.

(IoU) of [70%, 50%, 50%] in $[x, y, z]$ direction for *cars* and [50%, 50%, 50%] for *pedestrians* and *cyclists*. This stricter requirement emphasizes the improved accuracy of the detection position by dynamic motion handling as well as the performance in object height detection by a more significant difference between 3D and 2D Bird’s eye view (BEV) evaluation. The mean Average Precision (mAP) is the mean of the three class-wise APs. The results are specified for two different range regions, short-range (SR): evaluating all objects at distance of 0-30 m from the ego-vehicle and long-range (LR): evaluating all objects at distances >30 m. The symmetric Chamfer Distance (sCD) quantifies the distance between (static) points after ego-motion correction for two consecutive time steps and is used as a metric to represent the error of estimated ego-motion. Due to the noisy radar point cloud, this metric is calculated utilizing the lidar point cloud.

4.1 Ego-Motion Estimation Results

From Fig. 2, two categories of ego-motion patterns can be differentiated. Approaches resulting in a smooth motion estimation, EM-mG-Lidar and EM- v_{rr} , and algorithms with large deviations between frames. All deviating motion estimations show a similar pattern, most visible for the EM-G-Lidar estimated motion. This pattern repeats every 6 time steps. An explanation for this might be a time synchronization issue in data recording. This could also explain the apparent noise in the motion estimated from EM-P. Unfortunately, further investigations of this effect are impossible given the provided data. The amount of noise deviates between the different estimation strategies. Visual analysis shows that GICP-radar-based motion is most noise-prone. This can also be observed regarding the sCD

Table 1 3D object detection results on the VoD dataset quantified as mAP and sCD between the current point cloud and the ego-motion corrected point cloud from the previous time step. All results, irrespective of the ego-motion (EM) correction approach, are generated by applying PointPillars on radar data accumulated over 5 frames, ignoring the motion of dynamic objects. The best results are marked in **bold**. The arrow marks direction of better score.

EM estimation approach	sCD [m] ↓	mAP ↑			
		3D		BEV	
		SR	LR	SR	LR
No correction	0.285	32.0	10.1	42.9	22.6
EM-P	0.191	35.1	12.9	48.6	28.8
EM-G-Lidar	0.180	38.4	14.2	50.5	29.6
EM-mG-Lidar	0.235	33.5	9.4	46.3	24.8
EM-G-Radar	0.296	32.3	12.2	44.1	25.6
EM- v_{rr}	0.235	32.9	11.9	45.6	27.7
EM-PCAc	0.216	38.7	11.4	48.5	25.4

between time steps in Tab. 1. Employing EM-G-Radar for correction results in larger and therefore worse sCD compared to the uncorrected data. The EM-G-Radar reflects the time synchronization issue, and the inherent noisy measurements of the radar point cloud, which results in an insufficient correction in regard to the lidar point cloud, while still improving the object detection on radar data over no correction. The robust point matching utilized in PCAc yields a better motion estimation from the radar point cloud. It has a significantly lower sCD and higher mAP for the SR 3D-mAP but cannot reach the EM-P and EM-G-Lidar estimation performance. Comparing the sCD in Tab. 1

Table 2 3D object detection results on the VoD dataset quantified as mAP. All models, irrespective of the accumulation horizon are generated by applying PointPillars on radar data corrected by the EM-P approach and if applicable, dynamic objects were corrected by the baseline method Dyn-GT. The best results, of only ego-motion and the best considering dynamic motion correction are marked in **bold**.

Accumulation strategy	3D		BEV	
	SR	LR	SR	LR
1 scan	30.0	9.5	42.7	22.1
3 scans	35.9	12.8	47.2	26.9
5 scans	35.1	12.9	48.6	28.8
8 scans	35.7	12.0	49.1	26.4
10 scans	35.3	10.2	49.3	26.1
5 scans; Dyn-GT	36.3	13.5	47.6	27.1
10 scans; Dyn-GT	35.4	15.4	47.0	26.2

to the mAP shows that a low sCD corresponds to a better object detection performance. All approaches improve on the uncorrected baseline. For EM-mG-Lidar and EM- v_{rr} , it is observable that the performance is low compared to the other approaches. This strengthens the assumption that there is an inherent synchronization limitation.

4.2 Influence of the Accumulation Horizon

Different time horizons for point cloud accumulation are investigated to validate the aggregation with respect to the provided single frame data and to investigate the effects of longer time horizons for dynamic object handling. From Tab. 2, it is apparent that a large part of the improvement is already reached when accumulating just 3 frames. Accumulating more frames can result in better performance for some of the considered metrics but is diminished by worse performance in others. Accumulation over 5 frames balances good performance in SR and LR. This is especially apparent when the dynamic motion of objects is considered. A longer time horizon of 10 frames only improves the SR BEV performance, while in other cases, a shorter accumulation horizon results in better performance.

4.3 Learning-Based Estimation of Dynamic Motion and Consideration for the Accumulation

The evaluation in Sec. 4.1 has shown that the PCAc approach can estimate the ego-motion comparatively well, concluding that the PCAc approach works well on radar data too. Similar effects can be observed considering the instance association. Fig. 3 shows that the model can distinguish between different instances, but not all objects are detected correctly. For example, the model could not estimate the purple-colored object in Fig. 3a. The dark green colored object in Fig. 3a has been estimated correctly, but not all of the points that belong to the object are correctly predicted as part of an object. Above the light green object in Fig. 3a is another object (observable in camera data) that

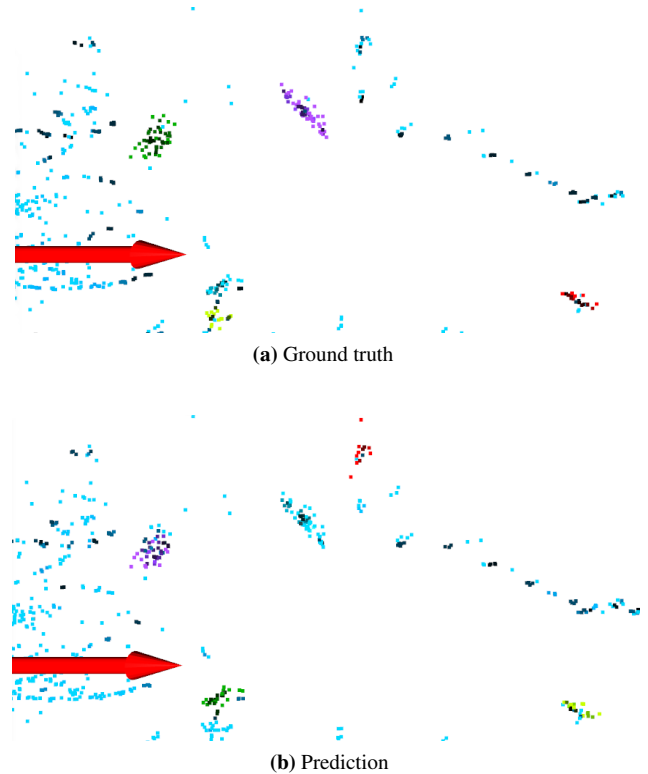


Figure 3 BEV perspective of the instance association on an accumulated point cloud. The ego-vehicle is located at the origin of the red arrow (outside of image). Blue: static points; points in other colors than blue belong to object instances and the same color indicates the same instance ID.

is not labeled but predicted in Fig. 3b. The red points in 3b are predicted as dynamic while not belonging to any object. These effects could be a result of imperfect labels. Similar effects can be observed for the VoD lidar data.

Utilizing the object motion for the separate treatment of dynamic objects in accumulated point cloud for object detection shows a clear advantage for all approaches in Tab. 3 over just considering the ego-motion in Tab. 1. The naive approach of correcting the motion by just using v_{rr} performs better than the label-based baseline. This could be due to errors in the motion estimation from the labels. PCAc yields the best results. This is partly due to the inherently improved ego-motion estimation, while the estimation of dynamic motion improves on the results from Tab. 1 in all metrics but the SR 3D-mAP measurement.

Table 3 3D object detection results on the VoD dataset quantified as mAP. All models, irrespective of the motion correction approach, are generated by applying PointPillars on radar data accumulated over 5 frames. The best results are marked in **bold**.

Dynamic motion estimation approach	3D		BEV	
	SR	LR	SR	LR
Dyn-GT	36.3	13.5	47.6	27.1
Dyn-PCAc	38.7	16.0	51.4	31.1
Dyn- v_{rr}	37.6	13.8	50.1	29.0

5 Conclusion

This work investigated the limitations of the VoD dataset for radar point cloud accumulation and approaches to mitigate missing ground truth ego-motion. It is shown that an improved ego-motion estimation improves the object detection performance. In addition to a better ego-motion estimation, a learning-based approach to mitigate the accumulation error for dynamic objects is applied to the dataset. Finally, it is shown that the motion of dynamic objects can be derived purely from the radar point cloud and that this improves object detection performance.

For future work, assuming a highly accurate inertial measurement-based ego-motion estimation will be available, the PCAc should be modified to utilize this motion instead of the estimated motion. This simplifies the architecture and might further improve the instance motion estimation. Furthermore, additional radar features like v_{rr} and the radar cross-section could be integrated into PCAc for better instance motion estimation. This could also lead to improvements of the ultimate task of 3D object detection. Eventually, the PCAc model and the object detector could be trained as a single end-to-end model to boost the detection performance further.

6 Literature

- [1] A. Palffy, E. Pool, S. Baratam, J. F. P. Kooij, and D. M. Gavrila, "Multi-class road user detection with 3+1d radar in the view-of-delft dataset," *IEEE Robotics and Automation Letters*, vol. 7, no. 2, pp. 4961–4968, 2022.
- [2] O. Schumann, M. Hahn, J. Dickmann, and C. Wöhler, "Semantic segmentation on radar point clouds," in *2018 21st International Conference on Information Fusion (FUSION)*, pp. 2179–2186, 2018.
- [3] Y. Long, D. Morris, X. Liu, M. Castro, P. Chakravarty, and P. Narayanan, "Full-velocity radar returns by radar-camera fusion," in *2021 IEEE/CVF International Conference on Computer Vision (ICCV)*, pp. 16178–16187, 2021.
- [4] A. Dewan, T. Caselitz, G. D. Tipaldi, and W. Burgard, "Rigid scene flow for 3d lidar scans," in *2016 IEEE/RSJ International Conference on Intelligent Robots and Systems (IROS)*, pp. 1765–1770, 2016.
- [5] X. Liu, C. R. Qi, and L. J. Guibas, "Flownet3d: Learning scene flow in 3d point clouds," in *2019 IEEE/CVF Conference on Computer Vision and Pattern Recognition (CVPR)*, pp. 529–537, 2019.
- [6] F. Ding, Z. Pan, Y. Deng, J. Deng, and C. X. Lu, "Self-supervised scene flow estimation with 4-d automotive radar," *IEEE Robotics and Automation Letters*, vol. 7, no. 3, pp. 8233–8240, 2022.
- [7] S. Huang, Z. Gojcic, J. Huang, A. Wieser, and K. Schindler, "Dynamic 3d scene analysis by point cloud accumulation," in *Computer Vision – ECCV 2022* (S. Avidan, G. Brostow, M. Cisse, G. M. Farinella, and T. Hassner, eds.), (Cham), pp. 674–690, Springer Nature Switzerland, 2022.
- [8] Y. Zhou, L. Liu, H. Zhao, M. López-Benítez, L. Yu, and Y. Yue, "Towards deep radar perception for autonomous driving: Datasets, methods, and challenges," *Sensors*, vol. 22, no. 11, 2022.
- [9] M. Meyer and G. Kuschik, "Automotive radar dataset for deep learning based 3d object detection," in *2019 16th European Radar Conference (EuRAD)*, pp. 129–132, 2019.
- [10] S. Baratam, "Radar-guided monocular depth estimation and point cloud fusion for 3d object detection," 2022.
- [11] A. Segal, D. Hähnel, and S. Thrun, "Generalized-icp.," in *Robotics: Science and Systems* (J. Trinkle, Y. Matsuoaka, and J. A. Castellanos, eds.), The MIT Press, 2009.
- [12] F. L. Markley, Y. Cheng, J. L. Crassidis, and Y. Oshman, "Averaging quaternions," *Journal of Guidance, Control, and Dynamics*, vol. 30, no. 4, pp. 1193–1197, 2007.
- [13] D. Kellner, M. Barjenbruch, J. Klappstein, J. Dickmann, and K. Dietmayer, "Instantaneous ego-motion estimation using doppler radar," in *16th International IEEE Conference on Intelligent Transportation Systems (ITSC 2013)*, pp. 869–874, 2013.
- [14] M. A. Fischler and R. C. Bolles, "Random sample consensus: A paradigm for model fitting with applications to image analysis and automated cartography," *Commun. ACM*, vol. 24, p. 381–395, jun 1981.
- [15] A. H. Lang, S. Vora, H. Caesar, L. Zhou, J. Yang, and O. Beijbom, "Pointpillars: Fast encoders for object detection from point clouds," in *2019 IEEE/CVF Conference on Computer Vision and Pattern Recognition (CVPR)*, pp. 12689–12697, 2019.
- [16] O. D. Team, "Openpcdet: An open-source toolbox for 3d object detection from point clouds," 2020.
- [17] P. Palmer, M. Krueger, R. Altendorfer, G. Adam, and T. Bertram, "Reviewing 3d object detectors in the context of high-resolution 3+1d radar," in *Accepted for publication on 2023 IEEE/CVF Conference on Computer Vision and Pattern Recognition Workshop on 3D Vision and Robotics (CVPRW)*, pp. 1–10, 2023.
- [18] L. N. Smith and N. Topin, "Super-convergence: very fast training of neural networks using large learning rates," in *Artificial Intelligence and Machine Learning for Multi-Domain Operations Applications* (T. Pham, ed.), vol. 11006, p. 1100612, International Society for Optics and Photonics, SPIE, 2019.
- [19] A. Geiger, P. Lenz, C. Stiller, and R. Urtasun, "Vision meets robotics: The kitti dataset," *The International Journal of Robotics Research*, vol. 32, no. 11, pp. 1231–1237, 2013.